Biomedical Signal Processing and Control 51 (2019) 328–337

Contents lists available at ScienceDirect

Biomedical Signal Processing and Control

journal homepage: www.elsevier.com/locate/bspc

P- and T-wave delineation in ECG signals using parametric mixture Gaussian and dynamic programming

Achuth Rao MV[a,*], Prakhar Gupta[b], Prasanta Kumar Ghosh[a]

[a] Indian Institute of Science, Bangalore, 560012, India
[b] National Institute of Technology, Tiruchirappalli, 620015, India

ARTICLE INFO

Article history:
Received 20 September 2018
Received in revised form 25 February 2019
Accepted 3 March 2019
Available online 15 March 2019

Keywords:
ECG
PT wave
Dynamic programming

ABSTRACT

Detection and tracking of the P- and T-waves are important issues in the analysis and interpretation of the ECG signals. This paper addresses the problem by using two mixture Gaussian function and the Dynamic programming. A key feature of the proposed algorithm is that it allows to incorporate the prior knowledge about the P/T wave location variations and robustness to errors in QRS detection. The proposed algorithm is evaluated on the annotated QT-database and compared against the algorithms based on differential evolution optimization strategy (DEOS) and generating blocks of interest (GBI). The experiments show that the proposed method determines the P- and T-peak locations with a root mean square error of 0.085 s and 0.091 s respectively. Both these values are better than the corresponding values from DEOS and GBI. Similarly, the proposed algorithm achieves a sensitivity of 96.13% and predictivity of 97.70%. While the predictivity is higher than both DEOS and GBI, the sensitivity is on par with GBOI and higher than that of DEOS.

1. Introduction

The analysis of electrocardiograms (ECGs) is used for diagnosing cardiac diseases. Most of the clinically useful information in ECGs can be obtained from the intervals, amplitudes and the shape of the ECG waveforms [1]. The development of accurate and robust methods for automatically extracting such waveform characteristics from ECG is a subject of major importance, especially for the analysis of long recordings [2].

The ECG captures the electrical activity on the skin as a result of the polarization and depolarization of the heart [3]. Normally this electrical activity is quasi periodic. Each period can be divided into four kinds of regions: P-wave, QRS-wave, T-wave and U-wave, where P-wave represents the atria depolarization, QRS-wave represents ventricles depolarization and T-wave represents ventricles repolarization [3]. U-wave typically has very low amplitude. The process of detecting the QRS wave is called QRS detection and the process of locating the P/T-wave start, end and peak points is called P/T-wave delineation.

Each cycle of ECG signal is composed of two parts. namely, QRS complexes and non-QRS regions as shown in Fig. 1. A QRS complex consists of Q, R, S waves. A non-QRS regions appears between two consecutive QRS complexes. Fig. 1 shows these two parts for three consecutive cycles of an illustrative ECG waveform. $\zeta_Q^i, \zeta_R^i, \zeta_S^i$ denote the time locations of the Q, R, S waves in the ith QRS complex. Typically the first step in an ECG signal analysis is the QRS detection followed by the P/T-wave delineation using the detected QRS wave. A QRS peak has high amplitude and is relatively easy to detect even in the noisy ECG signals compared to the P/T-waves. In this paper, we address the problem of locating the P/T-waves given the QRS-locations.

There are several P/T-wave delineation approaches in the literature [4]. The algorithms for P/T-wave delineation can be grouped into five categories. The first class of algorithms is based on adaptive filtering techniques proposed by Laguna et al. [5] and Takor et al. [4]. These algorithms perform bandpass filtering of the ECG signal and use thresholds to detect the P/T-waves locations. Strumillo et al. [6] proposed to use median filtering with different window sizes and the dominant peaks in the signal are preserved at all window sizes. Finally, based on the amplitudes of the peaks, the P/T waves are detected. Murthy et al. [7] proposed to filter the signal into different sub bands and use only few sub band signals to get the locations of the P/T-waves. But these algorithms are very sensitive to the thresholds used and there is no method to differentiate between the P/T/U-waves [8]. However, Elgendi et al. [9] have proposed an approach which performs bandpass filtering of the ECG signal followed by the usage of two moving average filters to delineate the P and T waves which, is less sensitive to thresholds and can distinguish between P/T/U-waves.

* Corresponding author.

https://doi.org/10.1016/j.bspc.2019.03.001
1746-8094/

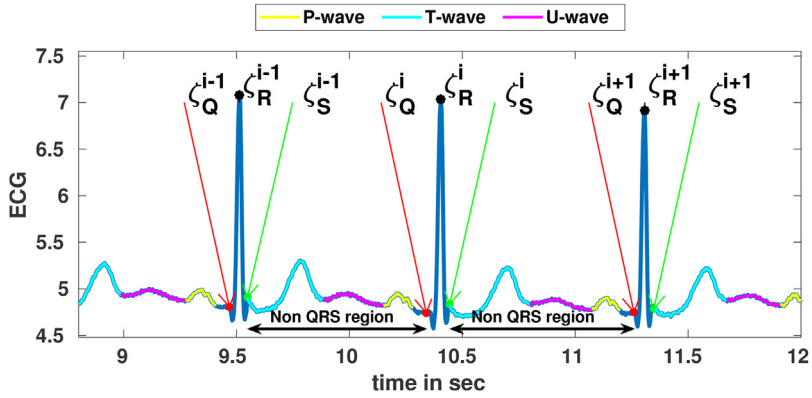

Fig. 1. Three consecutive cycles of a sample ECG. ζ_R^i, ζ_Q^i, ζ_S^i indicate the time locations of the peaks of the R-wave, onset of the Q-wave and end of the S-wave respectively in the ith ECG cycle. The P, T and U-waves within each non-QRS region are color coded.

The second class of methods decomposes the ECG signal into different basis functions and uses the basis weights to determine the locations of the P- and T-waves. Murthy et al. [10] observed that a two pole and two zero model can represent the discrete cosine transform (DCT) of a bell shaped bi-phasic function. The QRS, P/T-waves can be a single bell curve or biphasic and each wave is represented by a two pole and two zero model. The location of a P/T-wave is estimated by the pole and zero locations. Li et al. [8] and Martínez et al. [11,12] decomposed the ECG signal into different scales using the wavelet transform (WT) and the location of the P/T-wave is estimated by applying a threshold on the transformed signal at different scales. These algorithms are very sensitive to the model order selection when either P- or T-wave is absent [13]. The third class of approaches directly classifies the wave shapes or the features from the ECG signal using classification and pattern recognition methods, such as fuzzy theory [14], artificial neural networks [15], pattern grammars [16], and hidden Markov models [17]. There are several other delineation strategies including length transformation [18], uniform thresholding [19], approximating function theory [20], and characterization of TU complexes [13].

The fourth class of algorithms is based on the concept of fitting a model to the ECG waveform and extracting parameters from the model to determine waveform onsets and offsets. Clifford et al. [21] proposed a method to fit five mixture Gaussian function (GF) to the ECG signal whose parameters were estimated using nonlinear gradient descent. The mean parameters of the mixtures were used to identify the P/T-wave locations. Sayadi et al. [22,23] proposed to estimate these parameters using Kalman filters to exploit the dependency of parameters in the neighboring cycles. This results in a non-convex optimization problem, which is sensitive to the initial condition. Panigrahy et al. [24] proposed an approach involving template extraction followed by differential evolution for getting optimized parameters. This however, is a very computationally expensive approach. It should be noted that these approaches do not exploit any prior knowledge about the ECG signal which could potentially improve the P/T-wave localization.

The fifth class of algorithms includes non-parametric Bayesian methods proposed by Lin et al. [25,26]. This method assumes that the ECG wave is generated by filtering the impulses using an FIR filter. The impulse locations indicate the peaks of the P/T-waves. They also impose prior distributions on the locations of P/T-waves, for example on the distance between the consecutive P/T-waves. Prior information also includes assumptions that the P/T-waves are present in the first and second halves of an ECG cycle and the impulse response of the filter remains constant for few consecutive cycles. These prior distributions are combined with the likelihood of the observed data to obtain the posterior distribution of the unknown parameters. As there is no closed form solution for the parameter values which maximize the posterior distribution, authors use different variants of the Gibbs sampling method to get the samples of parameters given the ECG signal and the average of the samples is computed to get the locations of P/T-waves. It should be noted that there is no rule to detect the end and beginning of a P/T-wave. All of the above methods use some features of the wave such as low slope and low magnitude to detect the end and beginning of the P/T-wave [25]. In addition to the estimation of the wave peaks and limits (begin and end), an accurate waveform estimation is relevant for some medical diagnoses (such as T-wave alternans (TWA) detection [28]) or pathology analysis (such as arrhythmia detection [27]).

In this paper we propose a new algorithm that uses mixture Gaussian and dynamic programming for the P/T-wave delineation. Our formulation also allows easy inclusion of the prior information resulting in a tractable optimization problem. We assume that the shapes of both P- and T-waves follow Gaussian function. Thus, the non-QRS region is assumed to follow a two mixture Gaussian function (GF). We use a goodness of fit of the GF as a likelihood of occurrence of the P/T-waves and we also impose prior knowledge about the characteristics of ECG signal to achieve accurate delineation. Several model based approaches [21,23] for delineation use GF to model ECG waveform resulting in a non-convex optimization problem with many unknown parameters proportionate to the number of mixtures. Incorporating prior information in such cases makes the optimization even more challenging. Although we propose to use Gaussian mixture, we do not directly fit it to the ECG waveform. In particular, we use a two mixture GF reducing the number of unknown parameters in the optimization. We propose two kinds of prior on the locations of P/T-waves: The first prior is related to the smoothness of P/T-waves locations from cycle to cycle. We assume that the periodicity of the ECG signal does not change drastically from cycle to cycle and hence, the locations of P/T-waves in the neighboring cycles are correlated. Further, instead of assuming the occurrence of P/T-waves in two halves of an ECG cycle, we impose a soft prior on the P/T-wave locations, such that they are more likely to appear close to the R-peak. This makes the proposed algorithm robust to errors in R-peak location which, in turn, makes the tracking of P- and T-waves accurate even in the presence of dominant U-wave. Using the likelihood and the prior, a score function is constructed to find the optimal locations of the P/T-waves. We optimize the score function using dynamic programming. This method is referred as MGDP.

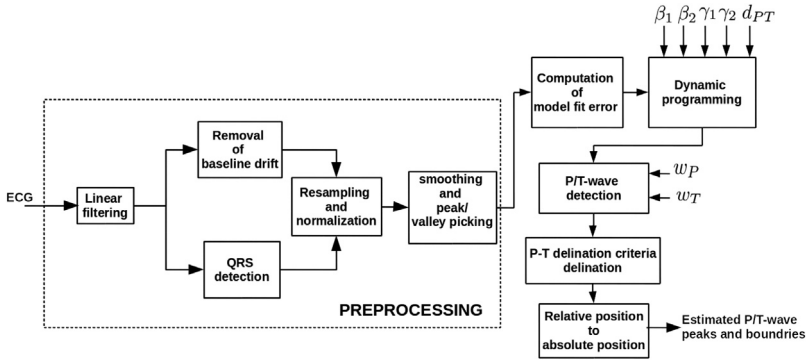

Fig. 2. Block diagram of the proposed P/T-wave delineation.

2. Proposed approach

The proposed P/T-wave delineation is performed in two main stages – (1) the first stage is a pre-processing step which removes the high frequency noise and motion artifacts and performs QRS detection, (2) the second stage locates the P/T waves using the mixture GF and dynamic programming. The block diagram summarizing these two stages is shown in Fig. 2. The details of each stage are explained below.

2.1. Preprocessing

As shown in Fig. 2, in the preprocessing step of the proposed P/T-wave delineation, we first detect QRS complexes and remove the baseline drift that occurs due to motion of electrodes or other low frequency noise. The linear filtering, removal of baseline drift and QRS detection are common preprocessing blocks in a P/T-wave delineation algorithm. The re-sampling of the non-QRS regions, normalization and smoothing are required for the proposed algorithm. Each block is briefly described below.

- Linear filtering: The ECG signal is filtered through a linear phase low pass filter. This is commonly used to remove the high frequency noise that can affect the QRS detection [29,30].
- Removal of baseline drift: Baseline drift causes inaccurate waveform estimation in the proposed algorithm. For this reason, we employ the method proposed by Chouhan et al. [30] to remove the baseline drift in each non-QRS region. This method first subtracts the median value of the signal from each sample followed by fitting a fourth degree polynomial to the whole signal using least square and subtracting it from the whole signal. The median value within each non-QRS region is corrected to get the baseline removed ECG signal. The resulting ECG signal is denoted by $ECG[n]$, where n denotes the sample index.
- QRS detection: QRS complexes are detected using the algorithm proposed by Pan et al. [29]. The ECG signal is passed though a bandpass filter to attenuate the noise. The resulting signal is passed though a differentiator followed by squaring and a moving window integration. The moving window integrator produces a signal with high value at R-peak because of its high slope and the value decays down from R-peak to Q-peak and S-peak that gives the locations of S-peak and Q-peak.[1]
- Re-sampling and normalization: The P- and T-waves appear in the non-QRS region. So we consider only the samples in the ith non-QRS region given by $ECG[n]$, $\zeta_S^{i-1} \leq n \leq \zeta_Q^i$ (as shown in Fig. 1). The number of samples in each non-QRS region is different and the number of samples in ith non-QRS region is denoted by $N_{RR}(i)$. But the proposed algorithm requires all non-QRS segments to have the same length $\mathcal{L}$. Hence we re-sample ith non-QRS region to a constant number ($\mathcal{L}$) of samples using the linear interpolation [33], which results in $z_i[n]$ for ith non-QRS region. We normalize samples in each non-QRS region by the amplitude of the R-peak that occurs before the non-QRS region to get $Z_i[n] = \frac{z_i[n]}{ECG[\zeta_R^{i-1}]}$. Following this, Z_i sequences for all non-QRS regions are stacked together to form a $\mathcal{L} \times N$ dimensional matrix $Z^N = [Z_1, Z_2, \ldots, Z_N]$, where N denotes the number of non-QRS regions in a given ECG signal.
- Smoothing and peak/valley picking: The proposed method requires a set of candidate locations for the P/T-waves. As P/T-waves occur only in non-QRS region, all samples in a non-QRS region can be given as the candidate locations for P/T-waves. But this increases the computational complexity of the proposed algorithm. We hypothesize that the actual P/T-waves are located at one of the local peaks or valleys in a non-QRS region. Hence, to reduce the computational complexity, the peaks and valleys in smoother version of ECG is provided as the possible candidate locations for the P/T-waves. The proposed approach needs the peaks of the original signal to be persevered after smoothing and hence, we use SGolay filter [34] of order 2 with a frame length of 101. The ith smoothed non-QRS region is denoted by $Z_i^S[n]$. Following this, the local minima and maxima of the resampled and smoothed ECG signal are found. The set of locations of valleys and peaks at ith non-QRS region is given to the proposed algorithm as the set of possible candidate locations for P/T-waves. This set is denoted by $\mathcal{K}_i$.

2.2. Proposed P and T peak tracking

Following pre-processing, the task of P/T-wave delineation becomes selecting the locations of P/T-waves in the ith non-QRS region from the set $\mathcal{K}_i$. We hypothesize that the P- and T-waves together in a non-QRS region follow a two mixtures GF with unknown means, variances and mixture proportions, Such a GF based approximation shown to be good in the work by Clifford et al. [21]. We use the inverse of the cost of fitting a two mixture GF as the likelihood of P/T-waves present at a given pair of locations when these locations are used as the means of two mixtures. We use two types of the prior information about the locations of the P/T-peaks. The first prior uses the fact that the location of the peak of P-wave in ith cycle is close to ζ_R^i and that of T-wave is close to ζ_R^{i-1}. The second prior assumes that the waveform shape of a non-QRS region doesn't change drastically from one cycle to the next, which, in turn, provides a smoothness constraint on the change in relative position of the P/T-peaks from one cycle to the next. From the likelihood and the prior probabilities, we construct a score function to be

[1] We experimented with other QRS detection algorithms [31,32] with no significant improvement over the one used.

maximized to find the optimal locations of the P/T-peaks. This maximization is performed efficiently using the dynamic programming technique.

2.2.1. Model fitting cost

Suppose it is given that the P/T-peaks are located at pth and qth samples of the ith non-QRS region ($p, q \in \mathcal{K}_i$). We fit a two mixture GF as shown below.

$$G(n, p, q) = \alpha_1 \mathcal{N}(n; p, \sigma_1) + \alpha_2 \mathcal{N}(n; q, \sigma_2), \quad 1 \le n \le \mathcal{L}, \tag{1}$$

where

$$\mathcal{N}(x; \mu, \sigma) = \frac{1}{\sqrt{2\pi\sigma^2}} e^{-\frac{(x-\mu)^2}{2\sigma^2}},$$

σ_1 and σ_2 are the variances of two mixtures. α_1 and α_2 are the respective weights of the mixtures. The parameters $\theta = \{\sigma_1, \sigma_2, \alpha_1, \alpha_2\}$ are obtained using gradient descent given the samples of $Z_i[n]$, $1 \le n \le \mathcal{L}$. Given the mixture GF mean locations p and q, the update equations[2] for $\sigma_i, \alpha_i, i = 1, 2$ are given in Appendix A.

To quantify the likelihood of locations of the P/T-wave at p and q in the ith non-QRS region, we use the inverse of goodness of fit of the mixture GF as follows:

$$L_i[p, q] = \left[\sum_{n=1}^{\mathcal{L}} \left\{ Z_i[n] - G(n, p, q) \right\}^2 \right]^{-1}, \quad p, q \in \mathcal{K}_i. \tag{2}$$

We normalize this pseudolikelihood for all combinations of locations ($\mathcal{K}_i$) to get the pseudoprobability mass function over variables p and q as follows:

$$L_i^N[p, q] = \frac{L_i[p, q]}{\sum_{p,q \in \mathcal{K}_i} L_i[p, q]}. \tag{3}$$

This allows us to combine this pseudoprobability mass function with the prior distribution on the locations of P/T-peaks as discussed in the following subsections.

2.2.2. Priors

The likelihood function obtained above (Eq. (3)) may not be sufficient to locate the P/T-peaks accurately because of the noise in the data and non-convexity of the MGF fitting. Hence we use two kinds of priors about the P/T-peaks in the ECG signals. Each of these priors is explained below.

a. The location of P-wave is typically close to the beginning of the Q wave and, similarly, T-wave is close to the end of S-wave. Due to such common patterns in the locations of P/T-waves, Lin et al. [25], for example, constrained the search region of P and T waves to be the first and last halves of a non-QRS region. This constraint may not be valid in all non-QRS segments as shown in a few illustrative ECG cycles in Fig. 3. Hence, in place of using a hard constraint, we use a soft prior on the locations of P/T-peaks by exploiting the statistical nature of their occurrences within a non-QRS region. We assume that the location of the T peak follows a β-probability density function (PDF), $M_T[n]$. Similarly, the PDF for the P peak location is denoted by $M_P[n]$ as follows:

$$M_T[n] = \frac{\frac{n}{\mathcal{L}}(1 - \frac{n}{\mathcal{L}})^{\beta_1 - 1}}{B(2, \beta_1)} \tag{4}$$

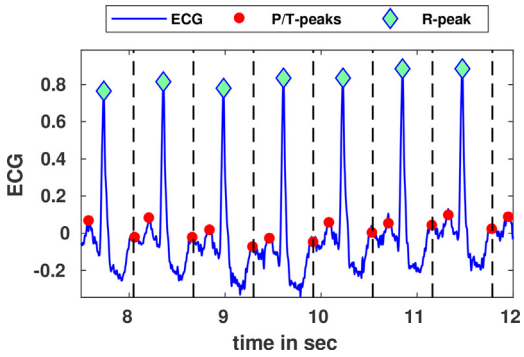

Fig. 3. Exemplary ECG cycles (sel48) highlighting the fact that the peak of a T-wave may not always be in the first half of a non-QRS region. The black dashed vertical lines indicate the mid point of the non-QRS regions.

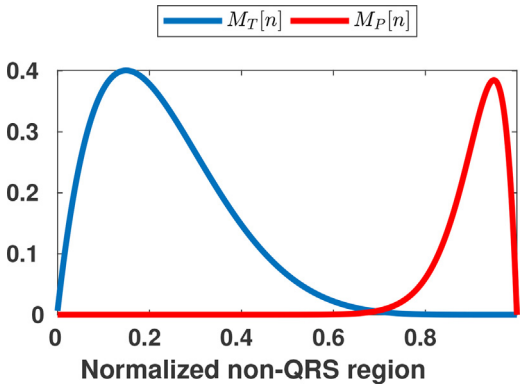

Fig. 4. Beta prior for peak location of P- and T-waves for $\beta_1 = 150$ and $\beta_2 = 50$.

$$M_P[n] = \frac{\left(\frac{n}{\mathcal{L}}\right)^{\beta_2 - 1}(1 - \frac{n}{\mathcal{L}})}{B(\beta_2, 2)} \tag{5}$$

where $0 \le n \le \mathcal{L}$, $B(a, b)$ is the beta function [35]. β_1, β_2 are the parameters of the prior distributions. Exemplary $M_T[n]$ and $M_P[n]$ representing ($\beta_1 = 150$ and $\beta_2 = 50$) the prior distribution of the locations of P/T-peaks in a normalized non-QRS region are shown in Fig. 4.

The β prior also makes the proposed method for P/T-wave delineation robust to the occurrence of the U-wave and the error in the estimate of the location of R peak. U-wave primarily occurs in the middle of a non-QRS segment between P- and T-waves. It could be dominant compared to each of P- and T-waves. While the goodness of fit of the two mixture GF could be erroneously high at the location of the U-wave, the location of the U-wave would have a low weight β-prior, because it is in the middle of the non-QRS region. This will reduce the chance of erroneously picking the U-waves in P/T-wave delineation. Similarly, if the location of the R peak is estimated wrongly, the actual R peak could appear in the very beginning or end part of a non-QRS region and the goodness of the fit could be high because of its high amplitude. However, the β prior helps in avoiding such erroneous R peaks since the β PDF has very small value when n is close to zero or $\mathcal{L}$.

b. It is known that the heart rate and also the locations of P/T-peaks do not change drastically from one cycle to the next [2]. We assume that better estimates of the P/T-peaks could be obtained by incorporating this smoothness in the peak locations across cycles. We quantify this smoothness constraint by defining a cost corresponding to the change in the relative positions of the P/T-peaks in the consecutive non-QRS regions. Suppose the locations

[2] Note that this optimization is different from the case where means of the Gaussian are included in the optimization variables along with variances and mixture weights which makes the objective function non convex and sensitive to the initial condition as suggested by Clifford et al. [21].

of the P/T-peaks are (p, q) and (p', q') in two consecutive non-QRS regions. Then the cost due to the smoothness is given by

$$M_{smooth}(p, q, p\prime, q\prime) = \frac{1}{\gamma_1\gamma_2 2\pi} e^{-\frac{(p-p\prime)^2}{2\gamma_1^2} - \frac{(q-q\prime)^2}{2\gamma_2^2}}, \quad (6)$$

where the γ_1 and γ_2 are the hyper parameters which control the smoothness of the P/T-peaks. It is clear that the cost M_{smooth} is high when there is small change in the P/T-peak locations in neighboring cycles maximizing which, in turn, encourages slow change of the P/T-peaks locations across ECG cycles.

2.2.3. Objective function

In the above subsections we discussed about the likelihood of P/T-peak locations, the priors on the locations of the P/T-peaks and the smoothness cost of P/T-peak locations in the consecutive non-QRS regions. Let N_c be the number of non-QRS regions in $ECG[n]$. For a given P/T-peak location at $x_j, y_j \in \mathcal{K}_j$ in the jth non-QRS region and $x_{j-1}, y_{j-1} \in \mathcal{K}_{j-1}$ in the $(j-1)$th non-QRS region, we define two kinds of costs for jth non-QRS region namely – within non-QRS region cost $\mathcal{C}_w(x_j, y_j)$ and across non-QRS regions cost $\mathcal{C}_a(x_j, y_j, x_{j-1}, y_{j-1})$ as follows

$$C_w(x_j, y_j) = L_j^N(x_j, y_j) M_T(x_j) M_P(y_j), \quad 1 \le j \le N_c \quad (7)$$

$$C_a(x_j, y_j, x_{j-1}, y_{j-1}) = \begin{cases} 1 & j = 1 \\ M_{smooth}(x_j, y_j, x_{j-1}, y_{j-1}) & 1 < j \le N_c \end{cases} \quad (8)$$

The total cost given the set of locations in each non-QRS region $\{(x_m, y_m) : 1 \le m \le N_c\}$ is defined as the sum of the cost at N_c non-QRS regions as follows:

$$C_{tot}(\{(x_m, y_m) : 1 \le m \le N_c\}) = \sum_{m=1}^{N_c} C_w(x_m, y_m) C_a(x_m, y_m, x_{m-1}, y_{m-1}) \quad (9)$$

The objective is to find the optimal set of indices's $\{(x_m^*, y_m^*) : 1 \le m \le N_c\}$ at each non-QRS region to maximize the total cost. The number of possible candidates for the P/T-peak locations can be further reduced by imposing the minimum distance constraint on the P/T-peaks $(y_m - x_m \ge d_{P,T})$ similar to [26]. Where $d_{P,T}$ denotes the minimum distance threshold found using the validation data.

$$\{(x_m^*, y_m^*) : 1 \le i \le N_c\} = \underset{\substack{\{x_m, y_m \in \mathcal{K}_m \\ (y_m - x_m) \ge d_{P,T} : \\ 1 \le m \le N_c\}}}{\arg\max} C_{tot}(\{(x_m, y_m) : 1 \le m \le N_c\}). \quad (10)$$

2.2.4. Dynamic programming

The solution to the objective function in Eq. (10) can be found by searching over all combinations of $(x_m, y_m) \in \mathcal{K}_m$ that results in $\prod_{i=1}^{N_c} |\mathcal{K}_i|^2$ number of evaluation of the objective function. However, the overall cost in the objective function in Eq. (10) is the sum of local costs which depend on the P/T-peak locations in two successive non-QRS regions. We exploit this nature of the cost in the objective function and solve the optimization using dynamic programming, whose steps are shown in Algorithm 1. The output of the algorithm (x_m^*, y_m^*) contains the locations of both P and T peaks in the mth non-QRS region which maximize the cost shown in Eq. (10).

2.2.5. P and T wave detection

The proposed algorithm estimates the best possible location of P-wave, irrespective of whether P-wave is present or absent in a given non-QRS region. It is observed that, in the absence of P-wave, the location estimated by the algorithm is closer to the Q-wave due to high β-prior, but the corresponding value of the α_2 is small. In the case of the T-wave, we observe similar trend. Hence, we develop criteria based on these observations to determine whether the P- and T- wave are present or not. We develop these criteria based on the (x_m^*, y_m^*), α_1 and α_2 values of the mixture GF at (x_m^*, y_m^*) separately for P- and T- waves. The criteria are given in Table 1. The criteria considers the presence of P- and T- waves when the normalized values of α_2 and α_1 are greater than a pre-defined thresholds W_P and W_T respectively.

Table 1
The P/T-waves detection criteria.

Class	Condition
P is present	$\frac{\lvert\alpha_2\rvert}{\lvert\alpha_1\rvert+\lvert\alpha_2\rvert} \ge W_P$
T is present	$\frac{\lvert\alpha_1\rvert}{\lvert\alpha_1\rvert+\lvert\alpha_2\rvert} \ge W_T$

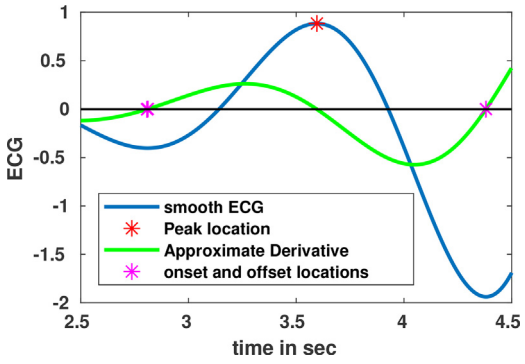

Fig. 5. A smooth P- or T-wave (blue curve) and its derivative (green curve) are shown. The zero crossings of the derivative are considered as the onset and end locations of the wave.

2.2.6. P and T wave delineation

Once we obtain the P/T-peaks, we propose a delineation criterion based on the preprocessed waveform, since there is no universal rule to locate the onsets and ends of P/T-waves. We compute an approximate derivative of the smooth signal $Z_i^S[n]$ using central difference $(\frac{Z_i^S[m+1]-Z_i^S[m-1]}{2*Ts}$, Ts is the sampling period) and find the locations where the derivative crosses zero around the locations of P/T-peaks. The location that is before the T-peak and that is closest to the R-peak is considered as the T-onset. The location that is after the T-peak is considered as T-end. Similarly, the P-onset and P-end are also obtained. This is illustrated in Fig. 5 for a synthetic wave.

2.2.7. Relative position to absolute position

The locations of P/T-peaks obtained by the dynamic programming (x_m^*, y_m^*) correspond to the locations on the re-sampled version of the non-QRS region. The locations are converted to their absolute values using the corresponding length of the non-QRS region $(N_{RR}(m))$ as given below.

$$\zeta_T^m = \zeta_S^{m-1} + \lceil \frac{x_m^* \times N_{RR}(m)}{\mathcal{L}} \rceil$$

$$\zeta_P^m = \zeta_S^{m-1} + \lceil \frac{y_m^* \times N_{RR}(m)}{\mathcal{L}} \rceil,$$

where $\lceil . \rceil$ indicates the nearest integer operation. ζ_T^m and ζ_P^m are used as the estimated P/T-peak locations. Similarly, the onsets and offsets of the P- and T-waves are also converted to their absolute locations.

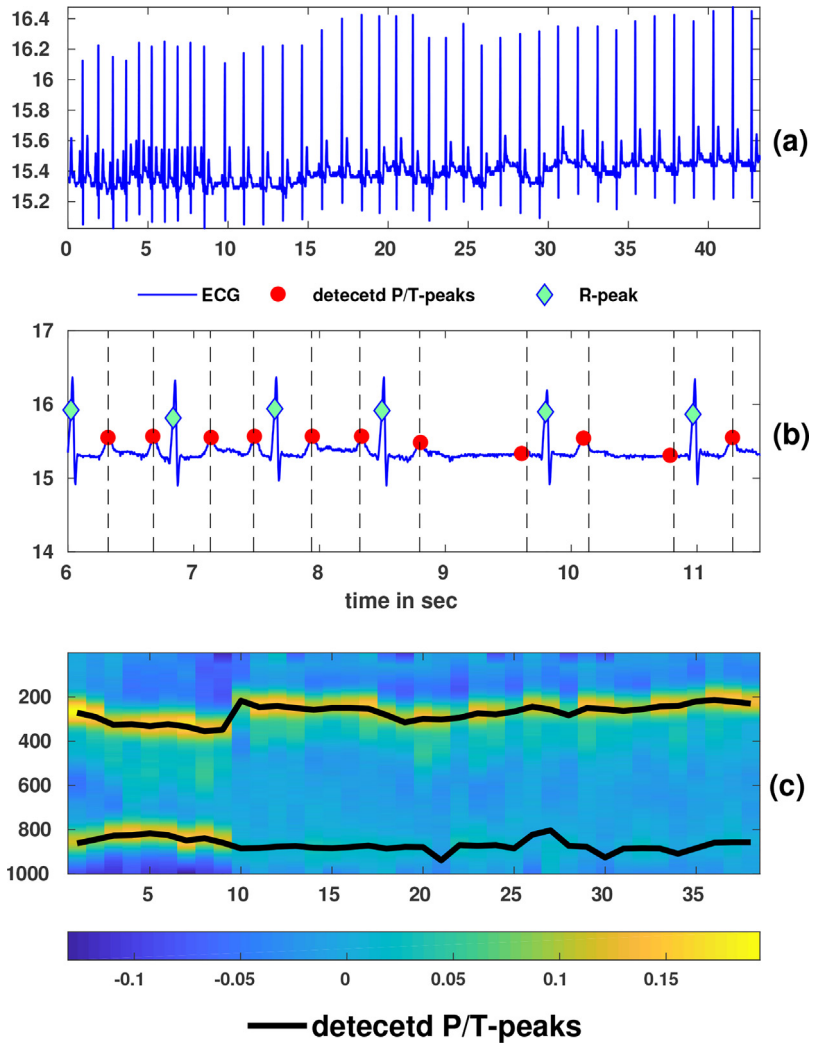

Fig. 6. Illustration of the P/T-delineation using MGDP. (a) ECG signal for sele0136. (b) Zoomed version of (a) to show the non-stationarity of ECG and the black vertical lines indicate the cardiologist annotation. (c) Resampled and normalized non-QRS regions Z^N with the estimated location of the peaks shown by the black lines.

Algorithm 1. Steps for solving Eq. (10) using dynamic programming

Initialization:
N_c = Numberofnon − QRSregions
$O_1(x, y) = C_w(x, y) \forall (x, y) \in \mathcal{K}_1$ (using Eq. (7))
for each non-QRS region of ECG l from 2 to N_c **do**
  $\forall x, y \in \mathcal{K}_l \quad and \quad (y - x) \geq d_{P,T}$, do
  $O_l(x, y) = \min_{(a,b)\in\mathcal{K}_{l-1}} \left\{ O_{l-1}(a, b) + C_w(x, y) C_a(x, y, a, b) \right\}$
  $k_l(x, y) = \underset{(a,b)\in\mathcal{K}_{l-1}}{arg\,\min} \left\{ O_{l-1}(a, b) + C_w(x, y) C_a(x, y, a, b) \right\}$
end for
Back tracking: $(x^*_{N_c}, y^*_{N_c}) = \underset{(a,b)\in\mathcal{K}_{N_c}}{arg\,\min} \left\{ O_{N_c}(a, b) \right\}$
for each non-QRS region l from $N_c - 1$ to 1 **do**
  $(x^*_l, y^*_l) = k_{l+1}(x^*_{l+1}, y^*_{l+1})$
end for

3. Experiments and results

3.1. Database and baseline scheme

We evaluate the ECG delineation algorithm using QTDB database [36]. This database includes the ECGs from two widely used databases – MIT-BIH arrhythmia database, the European ST-T database and several other ECG databases collected at Boston's Beth Israel Deaconess Medical Center. The additional recordings include extremes of cardiac (patho)physiology. It contains a total of 105 fifteen-minutes excerpts of two channel ECG signals sampled at 250 Hz and a total of 3170 beats (∼30–100 beats within each subject) was manually annotated by cardiologists, who identified the beginning, peak and end of the P-wave, beginning and end of the QRS-complex, the beginning, peak and end of the T-wave (if present), and the beginning, peak and end of the U-wave (if present). It should be noted that the QTDB has no annotated ECG cycle without a T-wave. We use only the first channel of ECG in all experiments in this work.

We compare the proposed algorithm with recent P/T-wave delineation methods, namely GBI [9] and DEOS [24]. They are shown to perform better than several ECG delineation techniques including those proposed by Sun et al. [37] and Sayadi et al. [23] respectively.

3.2. Evaluation

We evaluate the two main tasks in ECG delineation – P/T-wave detection and P/T-waves peak and boundary estimation using the following measures.

- We evaluate the P/T-wave detection accuracy by calculating the sensitivity $Se = TP/(TP + FN)$ and positive predictivity

P += $TP/(TP+FP)$, where TP denotes the number of true positive detections (wave is present and detected), FN stands for the number of false negative detections (wave is present but missed), and FP stands for the number of false positive detection (wave is not present but detected).

- We evaluate the P/T-waves peak and boundary estimation accuracy using root mean squared error (RMSE) between the ground truth location of peak or the boundary (f_k) and the estimated peak or the boundary location ($\hat{f}_k$). Following the work by Lin et al. [26], we also compute the mean (m) and standard deviation (s) as follows:

$$RMSE = \frac{1}{K}\sum_{k=1}^{K} e_k^2$$

$$m = \frac{1}{K}\sum_{k=1}^{K}(e_k), \qquad s = \frac{1}{K}\sum_{k=1}^{K}(e_k - m)^2$$

where $e_k = (f_k - \hat{f}_k)$ and K is the total number of annotated ground truth locations in the database.

- We evaluate the speed of P/T-wave delineation using relative computation time (RCT). It provides an indication of the speed of an algorithm and is computed as follows

$$RCT(\%) = 100\frac{CPU_{time}(s)}{duration_{ECG}(s)}$$

where $CPU_{time}(s)$ is the time in seconds taken by an algorithm and $Duration_{ECG}(s)$ is the duration of the ECG signal in seconds.

3.3. Experimental setup

1 Preprocessing: The ECG signal is filtered using a linear phase FIR filter to remove high frequency noise. The base line drift is removed using [30] and the QRS-waves are detected using the method outlined in [29]. The heart rate can go as low as 40 BPM. Thus, length of a non-QRS region can go as high as 375 samples. Hence, we decide to choose $\mathcal{L} > 375$. Each non-QRS region is resampled to the length $\mathcal{L} = 1000$. Each resampled non-QRS region is smoothed using SGolay filter of length 101 and order 2. A total of ten valleys and ten peaks (corresponding to the ten highest absolute amplitudes) are computed from every smoothed non-QRS region.

2 MGDP: The histograms of the ground truth locations of the P/T-peaks and U-wave in a normalized non-QRS regions are shown in Fig. 7. This shows that the beta prior for the P/T-peak location in a normalized non-QRS region could be a good fit. It also shows that the location variability for the T-peak is more than that of the P-peak. The U-wave appears to closer to the T-peak than the P-peak. The hyper parameters of the models are tuned using a validation set, 10% random subset of the annotated data, which is not used in the evaluation. The hyper parameters $d_{P,T} = 150$, $\beta_1 = 220$, $\beta_2 = 110$, $\gamma_1 = 80$ and $\gamma_2 = 80$ are found by minimizing the average RMSE error in the detected P/T-peak location. $W_P = 0.1$ is used to maximize the P-wave detection accuracy.[3]

3.3.1. One typical example

For illustration, the P/T-wave delineation is performed by applying the proposed MGDP method on the dataset "sele0136" of QTDB, a portion of which is shown in Fig. 6(a) and (b). This example has been chosen because signals from this data set contain sudden rhythm changes with obvious amplitude variations as shown in Fig. 6(b). From the figure it is clear that the wave peaks are detected accurately using MGDP in spite of sudden beat change. Fig. 6(c) shows the re-sampled and normalized matrix (Z^N) corresponding to the ECG signal. From Fig. 6(b), it is interesting to note that the P-waves are correctly detected even though their strength reduces significantly after fifth non-QRS region. This is mainly due to the maximization of the proposed score function that ensures smooth trajectories for the P- as well as T-wave that best fit every non-QRS region.

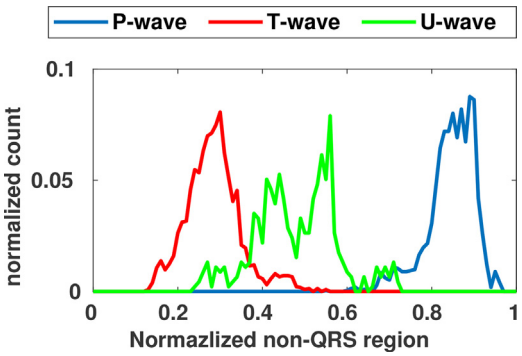

Fig. 7. Histogram of P-, T- and U-wave location in the normalized non-QRS region.

3.3.2. P- and T-wave delineation for different wave morphologies

We consider other illustrative examples, where, we evaluate the proposed algorithm on different wave morphologies that occur due to different clinical conditions four of which are shown in Fig. 8. It is clear from the figure that the MGDP is able to detect the P/T-peaks accurately in all four cases. For example, an inverted T-wave is present in the Fig. 8(a), a bi-phasic T-peak is present in Fig. 8(b) and (c); in spite of these morphological differences, the P/T-peaks are detected accurately. The P/T-peaks are detected accurately even in the presence of U-wave in Fig. 8(d)–(f), in spite of it being more dominant than the P/T-wave. It suggests that the two mixture GF assumption on the wave shapes is generic and also effective in detecting the P/T-peaks in case of different wave shapes.

3.3.3. Robustness to RR-peak error – an illustration

Most of the P/T-wave delineation methods [9] including the MGDP method requires a prior QRS detection. Error in the QRS detection can cause errors in P/T-wave delineation. To test the robustness of algorithm to QRS detection errors, we have added a random ±20 sample noise to the annotated QRS-peak locations and then detect the P/T-peaks using MGDP. The noisy R-peaks and the detection results are shown in Fig. 9(a). It is clear from the figure that the detected P/T-peaks are still accurate with the RR-peak error. This is because of the β prior which is low for the dominant peaks that appear near the boundaries of the non-QRS region. Most of the P/T peaks are detected correctly using MGDP, but the some of them are biased toward the R-peaks as shown in Fig. 9. The normalized matrix Z^N is also shown in 9 (b), where this biasness is clear near 30th–35th s. It is clear that due to the R-peak detection errors, the Z^N is affected only in the top and bottom rows. However, the MGDP does not select those high valued parts in the optimal trajectories for P/T-peaks.

3.4. Results and discussion

The P/T-wave detection Se and P+ are shown in Table 2. It should be noted that the QTDB has no annotated ECG cycle without a T-

[3] QTDB has no annotated ECG cycle without a T-wave, and, hence, the W_T threshold is not computed.

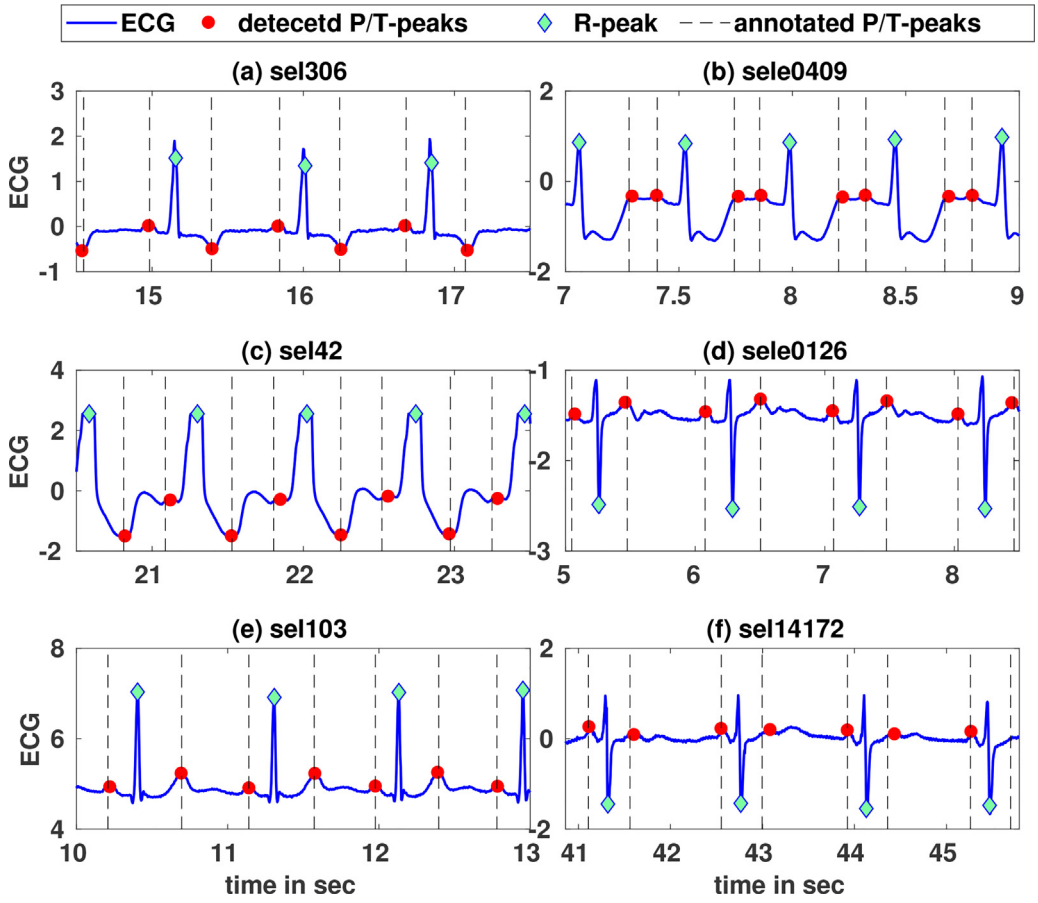

Fig. 8. Illustrative examples of P/T-delineation on ECG using MGDP for different wave morphologies. Black vertical lines indicate the locations from the cardiologist annotation of P/T-peaks. (a) sel306: Inverted T-wave that occurs due to myocardial ischaemia (b) sele409: biphasic T-wave where the T-wave appears in the middle of the non-QRS region (c) sel42: biphasic T-wave from a sudden death patient (d–f) sele0126,sel103,sel4172: ECG with U-wave due to hypokalaemia.

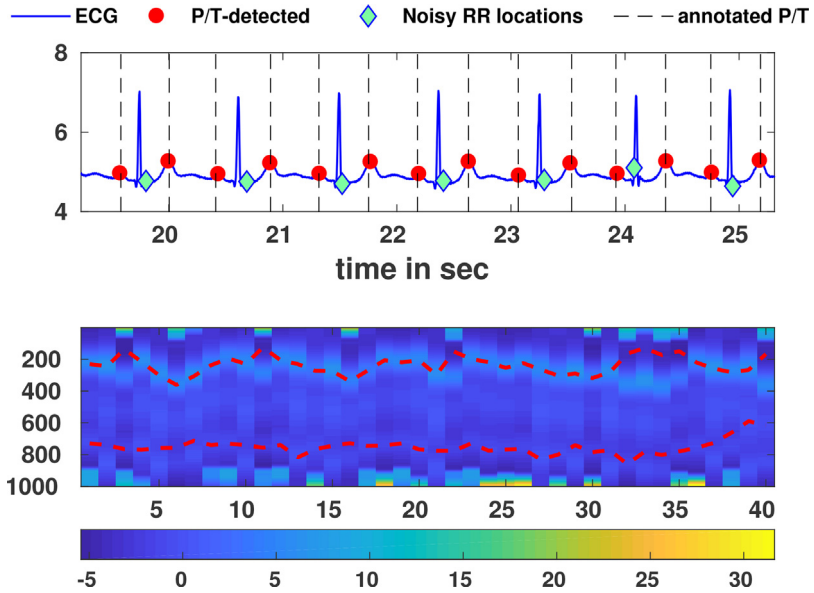

Fig. 9. Illustration of the robustness of the MGDP to error in R-peak detection. (a) Detected P/T-peak locations by MGDP when the detected R-peaks are erroneous. (b) The matrix Z^N with the detected P/T-peak locations shown by the dotted red lines.

wave. Hence we compute Se and P+ only for the P-wave. The MGDP outperforms DEOS and GBI in Se by 0.15% and 0.37% respectively. The MGDP outperforms DEOS and GBI in *P*+ by 0.66% and 0.77% respectively. We observe that MGDP is able to classify the presence or absence of P/T-peaks in the noisy conditions more accurately compared to the baseline schemes. The histograms of the $\frac{|\alpha_2|}{|\alpha_1|+|\alpha_2|}$

Table 2
Comparison of evaluation metrics for different methods in detecting P/T-peaks.

Method	RCT (%)	P-peak				T-peak			
		P+	*Se*	*RMSE*	$m \pm s$	*P+*	*Se*	*RMSE*	$m \pm s$
MGDP	67.18	**95.39**	**96.04**	**0.085**	**3.55(13.7)**	**100**	96.21	**0.091**	**3.65(10.25)**
DEOS	424.6	94.73	95.89	0.229	7.87(15.35)	**100**	94.82	0.127	7.20(14.65)
GBI	**24.63**	94.60	95.67	0.088	4.235(14.7)	**100**	**96.92**	0.231	13.09(25.0)

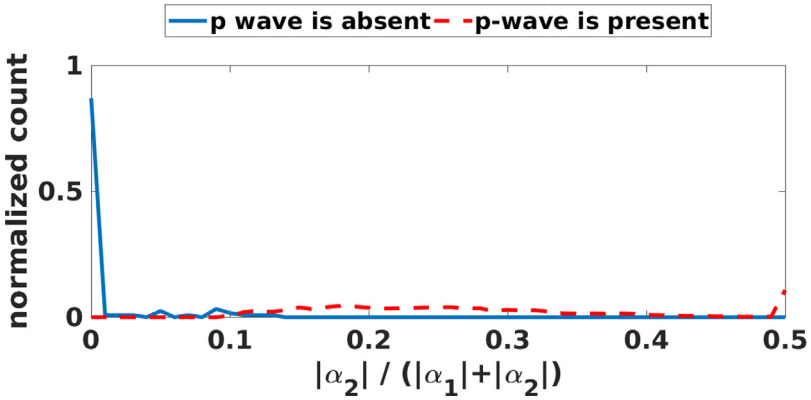

Fig. 10. Histogram comparison of $\frac{|\alpha_2|}{|\alpha_1|+|\alpha_2|}$ for a non-QRS region with and without P-wave.

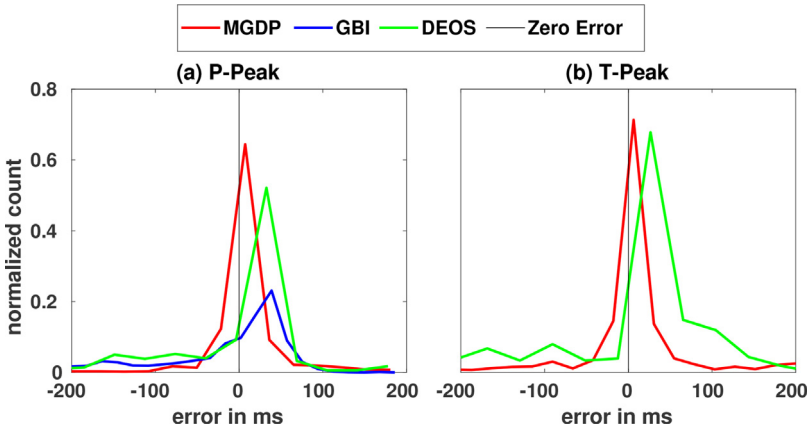

Fig. 11. Comparison of histogram of the error in estimating P/T-peaks for MGDP, DEOS and GBI. For T-peak the GBI excluded because of its large bias.

Table 3
Comparison of evaluation metrics for different methods in detecting P/T-boundaries.

Method	P_{on}		P_{end}		T_{on}		T_{end}	
	RMSE	$m \pm s$	*RMSE*	$m \pm s$	*RMSE*	$m \pm s$	*RMSE*	$m \pm s$
MGDP	**0.0861**	**63.7(30)**	**0.0645**	**58.4(13.5)**	**0.0928**	**64.2(29.8)**	**0.0560**	**48.8(38.4)**
DEOS	0.2126	158(52.9)	0.2200	124.1(83.1)	0.1937	135.95(69.6)	0.1083	92(39.6)
GBI	0.0976	78.9(26.3)	0.0970	68.2(33)	0.5949	259.00(119.3)	0.4249	179.9(83.3)

value for a non-QRS region with P-wave and without P-wave are shown in Fig. 10. It is clear from the figure that the values of $\frac{|\alpha_2|}{|\alpha_1|+|\alpha_2|}$ are well separated for these two classes.

The RMSE of estimating the P/T-peaks is also shown in Table 2. For P-peak, it is clear from the table that MGDP does better than both GBI and DEOS in terms of RMSE by 0.003 s and 0.1440 s respectively. Fig. 11(a) compares the histogram of error e_k for P-peak using different methods. It can be observed from the figure that for MGDP, the error is concentrated more around zero compared to DEOS. For DEOS, there is significant error around -150 ms, we observe that this happens due to detecting the dominant U-wave as P-wave. For T-peak, it is clear from the table that MGDP performs better than both GBI and DEOS in terms of RMSE by 0.14 s and 0.036 s respectively. From Fig. 11(b) it can be observed that there is a significant error around 100 ms for DEOS, this is because of error in detecting the dominant bi-phasic T-wave. The accuracy of detecting the P/T-wave boundaries is shown in Table 3. It is clear from the table that the MGDP performs better than both GBI and DEOS both in terms of RMSE and mean error. It is clear from the table that there is a large bias in the detection of the boundaries. We observe that the boundaries are mostly affected in case of bi-phasic T-wave, Q and S-waves and create a large bias.

Table 2 shows RCT(%) for different methods. It is clear from the table that the proposed method is 36% (absolute) more computationally complex than the GBI and less computationally complex than the DEOS. The RCT(%) of the proposed method is still less than 100% and, hence, it can be used for real time application.

4. Conclusion

This paper proposes a two mixture GF and dynamic programming based P/T-wave detection and delineation from ECG signal. It uses a prior about the P- and T-peak locations and uses a smoothness constraint on the location of P/T-waves across neighboring ECG cycles. We show that the proposed algorithm delineates the P/T-peaks accurately in different wave morphologies of the ECG signal. The prior on the location helps in detecting the T- and P- peaks accurately in the presence of U-wave and the RR peak errors. The proposed method is evaluated on the QTDB database and compared against the best of the recent algorithms, namely DEOS and GBI. We show the advantage of the proposed algorithm compared to both DEOS and GBI, particularly when the T-wave appears in the middle of a non-QRS region and the U-wave is dominant compared to the T-wave. The proposed algorithm also improves the P/T-peak detection and the P/T-wave delineation accuracy compared to both DEOS and GBI. The future work may include U-wave detection by using a 3 mixture GF and three dimensional dynamic programming, joint detection of PQRSTU-waves and extending the proposed algorithm to TWA detection using the α_1 value and the matrix Z^N.

Appendix A

A.1 Parameter update equation for two mixture GF

The nonlinear least square problem is given by

$$E(\alpha_1,\alpha_2,\sigma_1,\sigma_2;\mu_1,\mu_2) = \sum_{i=1}^{\mathcal{L}} \left(y_i - \alpha_1 e^{-\frac{(x_i-\mu_1)^2}{2\sigma_1^2}} - \alpha_2 e^{-\frac{(x_i-\mu_2)^2}{2\sigma_2^2}} \right)^2 \tag{11}$$

The gradients of the error function E with respect to σ_k and α_k for k=1,2 are given by

$$\frac{dE}{d\alpha_k} = -\sum_{i=1}^{\mathcal{L}} 2 \times \left(y_i - \alpha_1 e^{-\frac{(x_i-\mu_1)^2}{2\sigma_1^2}} - \alpha_2 e^{-\frac{(x_i-\mu_2)^2}{2\sigma_2^2}} \right) \times e^{-\frac{(x_i-\mu_k)^2}{2\sigma_k^2}}$$
$$\frac{dE}{d\sigma_k} = -\sum_{i=1}^{\mathcal{L}} \left(y_i - \alpha_1 e^{-\frac{(x_i-\mu_1)^2}{2\sigma_1^2}} - \alpha_2 e^{-\frac{(x_i-\mu_2)^2}{2\sigma_2^2}} \right) e^{-\frac{(x_i-\mu_k)^2}{2\sigma_k^2}} \frac{(x_i-\mu_k)^2}{\sigma_k^3} \tag{12}$$

The iterative update equations are given by

$$\alpha_{k+1} = \alpha_k - \omega \frac{dE}{d\alpha_k} \tag{13}$$

$$\sigma_{k+1} = \sigma_k - \omega \frac{dE}{d\sigma_k} \tag{14}$$

$\omega = 1e-3$ is used.

References

[1] P. Rautaharju, P. MacInnis, J. Warren, H. Wolf, P. Rykers, H. Calhoun, Methodology of ECG interpretation in the Dalhousie program; NOVACODE ECG classification procedures for clinical trials and population health surveys, Methods Inf. Med. 29 (4) (1990) 362–374.
[2] L. Smolarik, D. Mudroncik, L. Ondriga, ECG signal processing Advanced Materials Research, vol. 749, Trans Tech Publ, 2013, pp. 394–400.
[3] J.R. Hampton, D. Adlam, The ECG in Practice, Elsevier Health Sciences, 2013.
[4] N.V. Thakor, Y.-S. Zhu, Applications of adaptive filtering to ECG analysis: noise cancellation and arrhythmia detection, IEEE Trans. Biomed. Eng. 38 (8) (1991) 785–794.
[5] P. Laguna, R. Jané, P. Caminal, Automatic detection of wave boundaries in multilead ECG signals: validation with the CSE database, Comput. Biomed. Res. 27 (1) (1994) 45–60.
[6] P. Strumillo, Nested median filtering for detecting T-wave offset in ECGs, Electron. Lett. 38 (14) (2002) 1.
[7] I. Murthy, U. Niranjan, Component wave delineation of ECG by filtering in the Fourier domain, Med. Biol. Eng. Comput. 30 (2) (1992) 169–176.
[8] C. Li, C. Zheng, C. Tai, Detection of ECG characteristic points using wavelet transforms, IEEE Trans. Biomed. Eng. 42 (1) (1995) 21–28.
[9] M. Elgendi, M. Meo, D. Abbott, A proof-of-concept study: simple and effective detection of P and T waves in arrhythmic ECG signals, Bioengineering 3 (4) (2016) 26.
[10] I. Murthy, G. Prasad, Analysis of ECG from pole-zero models, IEEE Trans. Biomed. Eng. 39 (7) (1992) 741–751.
[11] J.P. Martínez, R. Almeida, S. Olmos, A.P. Rocha, P. Laguna, A wavelet-based ECG delineator: evaluation on standard databases, IEEE Trans. Biomed. Eng. 51 (4) (2004) 570–581.
[12] M. Yochum, C. Renaud, S. Jacquir, Automatic detection of P, QRS and T patterns in 12 leads ECG signal based on CWT, Biomed. Signal Process. Control 25 (2016) 46–52.
[13] J.A. Vila, Y. Gang, J.M.R. Presedo, M. Fernández-Delgado, S. Barro, M. Malik, A new approach for TU complex characterization, IEEE Trans. Biomed. Eng. 47 (6) (2000) 764–772.
[14] S. Mehta, S. Saxena, H. Verma, Recognition of P and T waves in electrocardiograms using fuzzy theory, 14th Conference of the Biomedical Engineering Society of India (1995) 2–54.
[15] E. de Azevedo Botter, C. Nascimento, T. Yoneyama, A neural network with asymmetric basis functions for feature extraction of ECG P waves, IEEE Trans. Neural Netw. 12 (5) (2001) 1252–1255.
[16] P. Trahanias, E. Skordalakis, Syntactic pattern recognition of the ECG, IEEE Trans. Pattern Anal. Mach. Intell. 12 (7) (1990) 648–657.
[17] J. Thomas, C. Rose, F. Charpillet, A multi-HMM approach to ECG segmentation, 18th IEEE International Conference on Tools with Artificial Intelligence (ICTAI) (2006) 609–616.
[18] F. Gritzali, G. Frangakis, G. Papakonstantinou, Detection of the P and T waves in an ECG, Comput. Biomed. Res. 22 (1) (1989) 83–91.
[19] V. Chouhan, S. Mehta, Threshold-based detection of P and T-wave in ECG using new feature signal, Int. J. Comput. Sci. Netw. Security 8 (2) (2008) 144–152.
[20] Z. Yang, L. Li, J. Ling, Approach to recognition of ECG P waves based on approximating functions, J. Biomed. Eng. 15 (2) (1998) 120–122.
[21] G. Clifford, M. Villarroel, Model-based determination of QT intervals, in: Computers in Cardiology, IEEE, 2006, pp. 357–360.
[22] O. Sayadi, M.B. Shamsollahi, Model-based ECG fiducial points extraction using a modified extended Kalman filter structure, First International Symposium on Applied Sciences on Biomedical and Communication Technologies (2008) 1–5.
[23] O. Sayadi, M. Shamsollahi, A model-based Bayesian framework for ECG beat segmentation, Physiol. Meas. 30 (3) (2009) 335.
[24] D. Panigrahy, P. Sahu, P and T wave detection and delineation of ECG signal using differential evolution (DE) optimization strategy, Aust. Phys. Eng. Sci. Med. 41 (1) (2018) 225–241.
[25] C. Lin, C. Mailhes, J.-Y. Tourneret, P- and T-wave delineation in ECG signals using a Bayesian approach and a partially collapsed Gibbs sampler, IEEE Trans. Biomed. Eng. 57 (12) (2010) 2840–2849.
[26] C. Lin, G. Kail, J.-Y. Tourneret, C. Mailhes, F. Hlawatsch, P and T wave delineation and waveform estimation in ECG signals using a block Gibbs sampler, IEEE International Conference on Acoustics, Speech and Signal Processing (ICASSP) (2011) 537–540.
[27] Z. Elghazzawi, F. Geheb, A knowledge-based system for arrhythmia detection, Computers in Cardiology (1996) 541–544.
[28] J.P. Martínez, S. Olmos, Methodological principles of T wave alternans analysis: a unified framework, IEEE Trans. Biomed. Eng. 52 (4) (2005) 599–613.
[29] J. Pan, W.J. Tompkins, A real-time QRS detection algorithm, IEEE Trans. Biomed. Eng. (3) (1985) 230–236.
[30] V. Chouhan, S.S. Mehta, Total removal of baseline drift from ECG signal, International Conference on Computing: Theory and Applications (ICCTA) (2007) 512–515.
[31] Z. Zidelmal, A. Amirou, M. Adnane, A. Belouchrani, QRS detection based on wavelet coefficients, Comput. Methods Programs Biomed. 107 (3) (2012) 490–496.
[32] S. Das, M. Chakraborty, QRS detection algorithm using Savitzky-Golay filter, Int. J. Signal Image Process. 3 (01) (2012) 55–58.
[33] M. Hazewinkel, Encyclopaedia of Mathematics: Coproduct Hausdorff Young Inequalities, vol. 2, Springer, 2013.
[34] S.J. Orfanidis, Introduction to Signal Processing, Prentice-Hall, Inc., 1995.
[35] J. Dutka, The incomplete beta functional historical profile, Arch. History Exact Sci. 24 (1) (1981) 11–29.
[36] P. Laguna, R.G. Mark, A. Goldberg, G.B. Moody, A database for evaluation of algorithms for measurement of QT and other waveform intervals in the ECG, in: Computers in Cardiology, IEEE, 1997, pp. 673–676.
[37] Y. Sun, K.L. Chan, S.M. Krishnan, Characteristic wave detection in ECG signal using morphological transform, BMC Cardiovasc. Disorders 5 (1) (2005) 28.